# The activity of the post-nova V1363 Cyg on long timescales

### Vojtěch Šimon<sup>1,2</sup>\*

<sup>1</sup> Astronomical Institute of the Czech Academy of Sciences, 25165 Ondřejov, Czech Republic <sup>2</sup> Czech Technical University in Prague, Faculty of Electrical Engineering, 16627 Prague, Czech Republic

\*E-mail: simon@asu.cas.cz

Received: Accepted

#### **Abstract**

V1363 Cyg is a cataclysmic variable (CV) and a post-nova. Our analysis of its long-term optical activity used the archival data from the AAVSO database and literature. We showed that the accretion disk of V1363 Cyg is exposed to the thermal-viscous instability (TVI) for at least part of the time. The time fraction spent in the high state or the outbursts dramatically changed on the timescale of decades. Highly variable brightness of V1363 Cyg displayed several episodes of a strong brightening (bumps in the light curve) from a cool disk in the TVI zone. In the interpretation, their vastly discrepant decay rates show that only some of these bumps can be attributed to the dwarf nova outbursts without strong irradiation of the disk by the hot white dwarf. The Bailey relation of the decay rate, if ascribed to a DN outburst of V1363 Cyg, speaks in favor of its orbital period  $P_{\rm orb}$  very long for a CV, about 20–40 hr. A dominant cycle length of about 435 d was present in the brightness changes all the time, even when the disk was well inside the TVI zone. We interpret it as modulation of the companion's mass outflow by differential rotation of the active region(s).

Key words: Accretion, accretion disks - novae, cataclysmic variables - Stars: individual: V1363 Cyg

#### 1 Introduction

Cataclysmic variables (CVs) are close binary systems in which matter transfers onto the white dwarf (WD) from its companion, a lobe-filling star (the secondary, the donor) (e.g., Warner (1995)). Their orbital periods  $P_{\rm orb}$  range from minutes to several days (Ritter & Kolb 2003). Various processes can be involved in the long-term activity of various CV types (e.g., Warner (1995)).

If the value of the time-averaged mass transfer rate  $\dot{m}_{\rm tr}$  between the donor and the non-magnetized accretor of a given CV accreting via the accretion disk is between some limits, the disk embedding the WD is exposed to the thermal-viscous instability (TVI) (Smak 1984; Cannizzo 1994; Hameury et al. 1998). It leads to episodic accre-

tion of matter from the disk onto the WD. The brightness of the optical, thermal emission of the disk increases by several magnitudes in such outbursts, typically lasting for days or weeks. Such CVs are called dwarf novae (DNe) (e.g., Warner (1995)). The TVI and the variations of  $\dot{m}_{\rm tr}$  between the components play a significant role in CVs' activity.

CVs called novalikes often possess the high states in which no outbursts occur. Their absolute magnitudes  $M_{\rm opt}$  are high, comparable to those of the DN outbursts or even higher (Warner 1987). Their accretion disks can be ionized in these hot states (Warner 1995). The variations of  $\dot{m}_{\rm tr}$  govern the changes of  $M_{\rm opt}$ .

The donor's magnetic activity can also influence the accretion disk structure (Pearson et al. 1997). It removes angular momentum from the disk material, increasing the

<sup>\*</sup> This research made use of the AAVSO database.

inward mass flow.

The magnetic field of the WD strongly influences the mass flow and activity of some CVs. Polars are CVs with so strongly magnetized WD  $(B>10^7 \,\mathrm{Gauss})$  that the accretion disk cannot form. Therefore, the matter flows directly to the caps at the magnetic poles of the WD. Various processes (cyclotron, bremsstrahlung) produce emissions of the accretion column of the matter accreting onto the WD (e.g., Warner (1995)). The high and low states typically last for weeks to months (e.g., Warner (1995)).

An explosion of a classical nova is caused by episodic hydrogen burning of the accreted matter on the WD (Bode & Evans 1989; Warner 1995). The source of nova can be either a CV with the accretion disk or a polar.

Extensive changes in the activity after the classical nova (CN) outbursts are observed in some CVs (Livio 1987). The features consistent with the DN outbursts (the TVI already operating) appear at least intermittently, mainly in the later phases (years, decades) of the slow decay of the luminosity of some post-novae (e.g., V446 Her (Stienon 1971; Honeycutt et al. 2011)). It suggests that they contain the accretion disks able to switch from the hot (ionized) state to the TVI regime on the timescale of decades.

V1363 Cyg (VV 279), classified as a DN in the catalog of Bruch et al. (1987), is a post-nova because it is approximately centered on a nebula with about 2 arcmin diameter, ascribed to the ejecta of a nova outburst (Sahman et al. 2015). The typical duration of the detectability of a nova shell is several centuries (Sahman et al. 2015), but it depends on several factors, e.g., on the distance of the nova. The distance of V1363 Cyg  $d=1693\pm146$  pc was determined from the observations by the satellite Gaia (Gaia Collaboration: Brown et al. 2018; Bailer-Jones et al. 2018)  $^1$ .

The photographic light curve of V1363 Cyg in 1948–1955 showed the variations probably caused by the DN outbursts and state transitions (Miller 1971). Szkody et al. (2014) detected quasi-periodic oscillations during the decline from a brightening (outburst) of V1363 Cyg. The spectrum of V1363 Cyg (Bruch & Schimpke 1992) showed strong Balmer emission lines with small decrement. They also identified a Na D absorption, which indicates the contribution of the secondary star both in the continuum and line emission. The continuum was inclined to the blue at short and the red at long wavelengths.

In this paper, we investigate the evolution of the longterm optical activity of V1363 Cyg. A preliminary version of this analysis was presented by Šimon (2021).



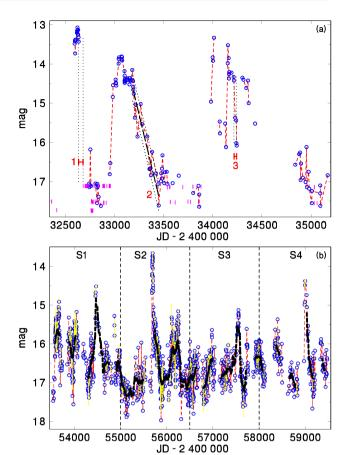


**Fig. 1.** The long-term light curves of V1363 Cyg. (a) Set A. Number 2 denotes the fit to the decaying branch of a long brightening and its standard deviation. Numbers 1 and 3 denote the limits of the steep decays. (b) Set B. The error bars of the 1-d means are marked, but they are often smaller than the size of the symbol. The points were connected by a line in the densely covered parts of the light curve to guide the eye. The black line marks the MAs for  $Q=40\,\mathrm{d}$ . The light curve was divided into four segments (S1 to S4). The distances between the ticks on the vertical axes are the same for both diagrams. See Sect. 3 for details. (This figure is available in color in electronic form.)

#### 2 Observations

The AAVSO International database (Massachusetts, USA)  $^2$  (Kafka 2019; Kafka 2021) contains both the visual and CCD measurements of V1363 Cyg. We used the V-band and unfiltered (with a sensitivity similar to the V-band) CCD data. The data obtained in these filters represented most of the CCD observations of V1363 Cyg. We included visual measurements to complete the coverage of the profile of a specific feature. They agreed with CCD data. The photographic data of V1363 Cyg published by Miller (1971) enabled us to extend the coverage of the light curve to the past.

<sup>2</sup> https://www.aavso.org/data-download

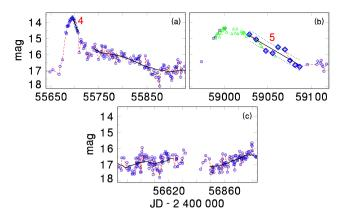


Fig. 2. (a) A bright outburst with a very long decay in V1363 Cyg. Circles represent the 1-d means of the AAVSO CCD V-band and unfiltered data. Also, the MAs of the outburst tail are shown. (b) A bright, well-defined outburst. The 1-d means of the AAVSO visual measurements (triangles) are included to cover the outburst profile. (c) Example of the segment and the MAs of the light curve without brightenings. The distances between the ticks on the vertical axes are the same for all diagrams. The straight lines with the standard deviation show the fits to the decaying branches (abbreviated as 4 and 5). See Sect. 3 for details. (This figure is available in color in electronic form.)

#### 3 Data analysis

#### 3.1 Overview of the activity

The long-term activity of V1363 Cyg was revealed to consist mainly of a series of large-amplitude fluctuations (set A (the 1-d means of the photographic data of Miller (1971)) in Fig. 1a and set B (the 1-d means of the V-band and unfiltered AAVSO data) in Fig. 1b). An inspection showed a typical uncertainty of a 1-d mean of set A was 0.1-0.2 mag. Regarding the AAVSO data in Fig. 1b, only the well-covered part of the light curve, abbreviated as set B, was selected. The coverage by the detections was dense, with only the short seasonal gaps. The dominant brightness variations occurred on the timescale of days and weeks. This segment is about twice longer than set A in Fig. 1a.

Usually, several CCD images of V1363 Cyg were obtained per night. The long series of more than 200 images were very few. We assessed how much such brightness changes affected the light curve on the timescale of days and longer. Therefore, we calculated the brightness means from the data points obtained in a given night. This approach enabled us to calculate the standard deviation of the brightness of such a night mean. We found that the scatter of the individual observations obtained in a given night was smaller than that occurring on the timescales of days and weeks (Fig. 1). The night means thus provided a good representation of the light curve on long timescales.

Most CCD observations of V1363 Cyg were obtained in the V-band, while Miller's (1971) photographic data band could be approximated by the B-band. Although we

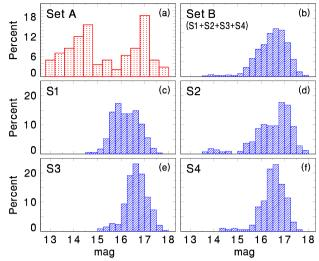


**Fig. 3.** Histograms of the brightness of V1363 Cyg in various time segments. (a) The photographic data from Fig. 1a (set A). (b) Set B (segments S1 to S4) of the AAVSO data from Fig. 1b. (c, d, e, f) Segments S1–S4. See Sect. 3 for details. (This figure is available in color in electronic form.)

compared the *B*-band light curve with that of the *V*-band, the peak-to-peak amplitude of the brightness variations was considerably higher than the possible changes of the color indices. The color variations were thus not expected to influence our results dramatically.

The two-sided moving averages (MA) of the brightness of CCD data were made to separate the long-term brightness variations from the superposed rapid (e.g., night-to-night) fluctuations. This method was described by Brockwell & Davis (1987). Various values of the filter half-width Q (in days) were tested. Figure 1b displays the light curve for  $Q=40\,\mathrm{d}$ , step  $10\,\mathrm{d}$ . The MAs were interrupted in the seasonal gaps and their vicinity. Also, the sharp peaks of some strong brightenings (Fig. 2) were omitted from this fitting because  $Q=40\,\mathrm{d}$  yielded a good fit to the relatively gradual variations but not to the occasional sharp peaks.

Figure 2 shows the examples of the features of the light curve of V1363 Cyg. The very bright outbursts in Figs. 2a and 2b differ from each other by the profile of the decaying branch (a very long one with strong undulations is displayed in Fig. 2a). Figures 2c and 2d show the examples of the complicated light curve of V1363 Cyg in the time segments without intense brightenings. The "quiescent" levels (plateaux) can attain various brightnesses.

The histograms of the brightness of V1363 Cyg in various time segments are displayed in Fig. 3. The histogram for set A from Fig. 1a was compared with that for set B from Fig. 1b. The upper limits in the photographic data could only influence the brightness lower than 17 mag. Further, the whole set B was divided into four segments

S1–S4 to assess the time evolution of the brightness in Figs. 3cdef.

A comparison with histogram for brightnesses of set A shows a big difference in a part of the brightness higher than 15 mag. In this brightness range, Fig. 3a contains a big bump where Fig. 3b displays only a long tail.

The histogram for the brightnesses of set B usually consists of a broad, asymmetric bump. The prominence of the tail toward the higher magnitudes varied for the individual time segments. A very prominent tail was present in segment S2.

The fits to the decays of the brightenings numbered as 1–5 in Figs. 1a and 2, supplemented by the upper limits in the fragmentary data, enabled us to determine their decay rates  $\tau_D$  (in d mag<sup>-1</sup>). They served the analysis of the nature of these events, discussed in Sect. 4. A comparison of the decaying branches of these brightenings with those of DNe is shown in Fig. 4;  $\tau_D$  is plotted versus  $P_{\rm orb}$ . It enables us to discuss the properties of the episodic brightenings (outbursts). Moreover, an assessment of whether the Bailey relation of DN outbursts (Bailey 1975) applies to any of them can be made. Although the coverage of some events is too fragmentary to obtain reliable values of  $\tau_D$  of their decays, even the upper limits of the decay rate enable us to show the broad range of  $\tau_D$  in V1363 Cyg.

The data in Fig. 4 come from Warner (1995), Šimon (2000a) (DO Dra), Šimon (2000b) (DX And), Shears & Poyner (2010) (V630 Cas), Šimon (2018) (X Ser), AAVSO database (Kafka 2021) (V392 Per, UY Pup). Please note that the values of  $\tau_{\rm D}$  of DO Dra and GK Per are smaller than in most DNe with the comparable  $P_{\rm orb}$ . For GK Per, only the steepest part of the decline was used for the determination of  $\tau_{\rm D}$  (Šimon 2018). These two CVs are known to be the intermediate polars, according to Patterson et al. (1992) and Watson et al. (1985).

The horizontal lines in Fig. 4 denote the values of  $\tau_{\rm D}$  of events 1–5 of V1363 Cyg from Figs. 1a and 2. The belt of  $\tau_{\rm D}$  of DNe (diamonds, circles, crosses), spanning between  $P_{\rm orb}$  of 1.1 hr and 137 hr, indicates the length of  $P_{\rm orb}$  of V1363 Cyg bigger than about 20 hr if its brightening episodes with the smallest  $\tau_{\rm D}$  (events 1, 3, and 4) are the DN outbursts obeying the Bailey relation (Bailey 1975).

#### 3.2 Time variations

A search for periods in the brightness variations in Fig. 1b used the Lomb-Scargle method (Lomb 1976), included in the code Peranso<sup>3</sup>. The 1-d means of the brightness from Fig. 1b) were used (Fig. 5a).

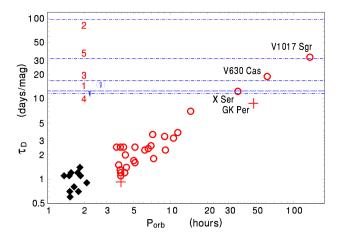


**Fig. 4.** The decay rate of DN outbursts,  $\tau_{\rm D}$ , versus  $P_{\rm orb}$ . DNe below and above the period gap (e.g., Warner (1995)) are marked by the diamonds and circles, respectively. Crosses mark the intermediate polars (see Warner (1995) for definition). The horizontal lines with the numbers denote the values of  $\tau_{\rm D}$  of the decays of events 1–5 in Figs. 1a and 2. See Sect. 3.1 for details

We found the modulation with the period (cycle-length) CL of about 435 d. The folded light curve of the 1-d means in Fig. 5b is gradual, roughly symmetric. For comparison, a period search of the data with brightnesses lower than 15.2 mag to avoid flares was made. The resulting periodograms are included in Fig. 5a. Both the periodograms and the folded light curves are mutually similar for both sets (Fig. 5).

## 3.3 V1363 Cyg in the context of the CV absolute magnitudes

Figure 6 shows the position of V1363 Cyg in the absolute optical magnitude  $M_{\rm opt}$  vs.  $P_{\rm orb}$  diagram of CVs with accretion disks. The range of  $M_{\rm opt}$  similar to that of V1363 Cyg in various stages of its activity is plotted. Table 1 summarizes the parameters of these CVs. The values of their d were determined from the observations by ESA Gaia (Bailer-Jones et al. 2018) <sup>4</sup>. Extinction  $A_V$  mainly was determined from the 3D map of Galactic reddening <sup>5</sup> of Green et al. (2018).

The zone below maxima's peaks of outbursts of DNe (Patterson 2011) represents the region in which the accretion disks are exposed to the TVI. Also, the minimum and maximum magnitudes of several DNe (as the AAVSO light curves show) with  $P_{\rm orb}$  longer than those in Patterson (2011) are displayed in Fig. 6 for comparison. These peak magnitudes enable us to extend the TVI region to  $P_{\rm orb}$  longer than used by Patterson (2011). An extension of his fit from the 6–8 hr region to the longer  $P_{\rm orb}$  shows that

<sup>3</sup> www.peranso.com

<sup>4</sup> http://vizier.cfa.harvard.edu/viz-bin/VizieR?-source=I/347

<sup>&</sup>lt;sup>5</sup> http://argonaut.skymaps.info/

**Table 1.** Parameters and types of CVs used in Fig. 6. These objects are arranged according to the length of  $P_{\rm orb}$ . N is nova, RN is a recurrent nova, NL is novalike, VS is V Sge-type, DN is dwarf nova, UG is DN of the U Gem type, UGZ is DN of the Z Cam-type. LC refers to the sources of the light curves for Fig. 6. The lengths of  $P_{\rm orb}$  are measured in hours. The highest and the lowest apparent magnitudes are abbreviated as  $mag_{\rm max}$  and  $mag_{\rm min}$ . They refer to the pre-nova or post-nova. The highest and the lowest absolute magnitudes are abbreviated as  $M_{\rm max}$  and  $M_{\rm min}$ . Distance, denoted as d, is given in parsecs. Extinction measured in magnitudes is abbreviated as  $A_V$ . See Sect. 3.3 for details. \*

Name	Type	LC	$P_{\rm orb}$ (hr)	$mag_{\max}$	$M_{\rm max}$	$mag_{\min}$	$M_{\min}$	d	$A_V$
GQ Mus	N(LO83),NL(AAVSO)	AAVSO	1.425  DS89	18.2	5.0	18.9	5.7	2456	1.2 K84
BK Lyn	N(H58), NL, DN (P13)	P13	1.7995 R96	13.6	5.1	16.0	7.5	498	0
$V1974\mathrm{Cyg}$	N(C92),NL?(SC10)	AAVSO	1.9503 D94	16.8	5.2	17.6	6.0	1568	0.6
$V382\mathrm{Vel}$	N(G00),NL(AAVSO)	AAVSO	3.5076  B01	16.0	4.5	16.5	5.0	1707	0.3 D02
$\operatorname{CT}\operatorname{Ser}$	N(M48),NL(R05,CRTS)	CRTS	4.68  R05	16.1	3.4	16.8	4.1	3453	0.01
$V446\mathrm{Her}$	N, NL(S71), UG(H11)	H11	4.97  TT00	15.1	3.5	17.1	5.5	1308	1.0
$V617\mathrm{Sgr}$	VS(SD98)	AAVSO	4.9718 C99	14.5	-0.9	16.4	1.0	9539	0.5
WX Cen	VS(SD98)	AAVSO	10.0 DS95	12.7	-0.7	14.3	0.9	2699	$1.2~\mathrm{SD98}$
Q Cyg	N, NL(K03)	AAVSO	10.08  K03	14.2	3.0	15.3	4.1	1320	$0.6~\mathrm{KS}11$
VSge	NL(H65), VS(SD98)	AAVSO	12.3406  H65	9.9	-2.5	12.2	-0.2	2236	0.7
BV Cen	DN(B74)	AAVSO	14.631  VB80	11.1	2.9	13.2	5.0	363	0.4  W880
QR And	SX,NL(GW95)	GW95	15.85 B95	11.6	0.1	12.5	1.0	1857	0.2
USco	RN(W81)	AAVSO	29.5335  SR95	17.6	2.8	18.4	3.6	6559	0.74  P15
XSer	N(L08,D81,D90),NL(H98),UG(S18)	S18	35.472  TT00	14.2	1.3	17.2	4.3	3056	0.5
$\operatorname{GK}\operatorname{Per}$	N(SB83),NL,UG(SB83,H81)	S02	47.76 C86	10.3	1.4	13.2	4.3	437	0.7
$V630\mathrm{Cas}$	UG(S17,SP10)	SP10	61.5329 O01	13.9	1.0	16.2	3.3	3004	0.5
$V392\mathrm{Per}$	N,NL(M20),UG(AAVSO)	AAVSO	81.8832  M20	13.5	-1.3	16.9	2.1	3416	2.1
$\rm V1017Sgr$	UG,N(M46)	M46	138.144  S17	10.9	-0.1	14.3	3.3	1227	0.6
$V1363\mathrm{Cyg}$	UGZ(M71,AAVSO)	AAVSO		13.7	1.6	17.8	5.7	1693	1.0

\* References: LO83: Liller & Overbeek (1983); AAVSO (Kafka 2021); DS89: Diaz & Steiner (1989); K84: Krautter et al. (1984)); H58: Hsi (1958); P13: Patterson et al. (2013); R96: Ringwald et al. (1996); C92: Collins et al. (1992); SC10: Schaefer & Collazzi (2010); D94: De Young & Schmidt (1994); G00: Garcia (2000); B01: Bos et al. (2001); D02: Della Valle et al. (2002); M48: McLaughlin (1948); R05: Ringwald et al. (2005); CRTS: Drake et al. (2009); S71: Stienon (1971); H11: Honeycutt et al. (2011); SD98: Steiner & Diaz (1998); C99: Cieslinski et al. (1999); DS95: Diaz & Steiner (1995); K03: Kafka et al. (2003); KS11: Kolobow & Sion (2011); H65: Herbig et al. (1965); B74: Bateson (1974); W880: Williger et al. (1988); GW95: Greiner & Wenzel (1995); B95: Beuermann et al. (1995); W81: Williams et al. (1981); SR95: Schaefer & Ringwald (1995); P15: Pagnotta et al. (2015); L08: Leavitt (1908); D81: Duerbeck (1981); D90: Duerbeck & Seitter (1990); H98: Honeycutt et al. (1998); S18: Šimon (2018); T700: Thorstensen & Taylor (2000); SB83: Sabbadin & Bianchini (1983); H81: Hudec (1981); S02; Šimon (2002); C86: Crampton et al. (1986); S17: Samus et al. (2017); SP10: Shears & Poyner (2010); O01: Orosz et al. (2001); M20: Munari et al. (2020); M46: McLaughlin (1946); S17: Salazar et al. (2017); M71: Miller (1971);

all CVs in Fig. 6 lying below it are in the TVI region. Only the outburst peak of V392 Per may approach its limit.

Figure 6 also shows post-novae of various types with  $M_{\rm opt}$  in the zone of brightnesses similar to that of V1363 Cyg. The X symbols in Fig. 6 denote the states of activity of the post-novae X Ser (Honeycutt et al. 1998) and GK Per (Kafka 2021), in which the quiescent level was brighter than usual, and the DN outbursts were suppressed or absent. The recurrent nova U Sco inside the TVI region displays no DN outbursts (Kafka 2021). The DN outbursts of V392 Per and V1017 Sgr were observed only before their CN outbursts (AAVSO; McLaughlin (1946)). V1363 Cyg itself is situated in the TVI region in quiescence (near min. brightness) irrespective of its  $P_{\rm orb}$ .

#### 4 Discussion

We present an analysis of the long-term optical activity of the post-nova V1363 Cyg. We show that its disk is exposed to the TVI at least near the minimum brightness. The time fraction spent in the high state or the outbursts dramatically changed on the timescale of decades, as shown by a comparison of the histogram for the brightness of set A with those for set B (Fig. 3).

We interpret the histogram of the brightness in set B (Fig. 3), consisting of a broad bump with a long tail toward the higher brightness, as the fluctuations and occasional brightenings from a cool disk in the TVI zone. The value of  $M_{\rm opt}$  in the outburst peak of V1363 Cyg speaks in favor of  $P_{\rm orb} > 12\,\rm hr$ , as indicated by the peak magnitudes of the DN outbursts in Patterson (2011) (Fig. 6).

The detectability of the secondary as the NaD absorp-

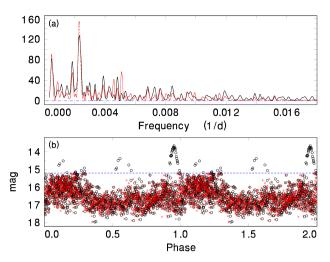
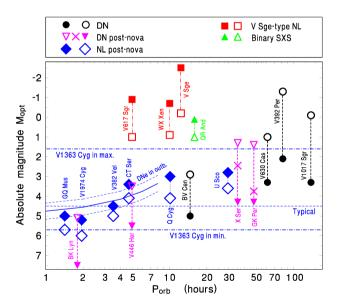


Fig. 5. Periods CL of the brightness variations in V1363 Cyg. The data were investigated with the Lomb-Scargle method (Lomb 1976). (a) Periodogram for the 1-d means of the brightness (a solid line). The red dashed line denotes a periodogram for the data with brightness lower than 15.2 mag to avoid flares. (b) The 1-d means of the brightness folded with  $CL=434.8\,\mathrm{d}$  (the highest peak of the solid line in panel (a)). The red x denotes the data with brightness lower than 15.2 mag folded with  $CL=436.3\,\mathrm{d}$  (the highest peak of the red dashed line in panel (a)). The starting point of the folding is the start of both data sets in JD 2453 541.8 in Fig. 1b. The folded light curve is plotted twice. See Sect. 3 for details. (This figure is available in color in electronic form.)



**Fig. 6.** The positions of V1363 Cyg (magnitudes in CCD data) in the  $M_{\rm opt}$  versus  $P_{\rm orb}$  diagram. Its maximum and minimum values of  $M_{\rm opt}$  are given. The typical  $M_{\rm opt}$  of V1363 Cyg corresponds to the peak of the bump in the histogram in Fig. 3b. The maximum and the minimum magnitudes (except deep eclipses in U Sco (Schaefer & Ringwald 1995)) of CVs are displayed. The solid blue line represents maxima's and supermaxima's peaks of DNe with  $P_{\rm orb} \leq 8\,{\rm hr}$  (Patterson 2011). The dashed lines denote the standard deviation. The meanings of the symbols are given in the legend (they include the observed outbursts of DNe with  $P_{\rm orb}$  longer than those in Patterson (2011). See Sect. 3 and Table 1 for details. (This figure is available in color in electronic form.)

tion (Bruch & Schimpke 1992) speaks in favor of  $P_{\text{orb}}$  of V1363 Cyg considerably longer than the period gap (e.g., Dantona & Mazzitelli (1982)). A contribution of the secondary component to the light curve profile may be significant, especially near the lower part of the histograms in Fig. 3. Since the brightness of V1363 Cyg only seldom achieves its lowest level, V1363 Cyg appears to be active all the time. The value  $M_{\rm min} \approx 5.7$  (Table 1) shows that if the fluxes of the secondary and the disk are mutually comparable in this epoch, the position of V1363 Cyg in Fig. 6 may be similar to that of BV Cen with a G5-G8 IV-V secondary (Vogt & Breysacher 1980). As regards the luminosity of this component, the current type of CV is determined by its previous evolution (Podsiadlowski et al. 2003). The spectra of V1363 Cyg, especially in its low brightness seasons, can help.

A dominant cycle-length of about 435 d, much longer than the superposed features like outbursts, was present in the light curve of V1363 Cyg all the time in set B, even when the disk was well inside the TVI region. The outbursts or flares occurred irrespective of the phase of this cycle (Fig. 5). In the interpretation, it can be caused by the appearance and changes of the position of the active regions (loops (Kafka et al. 2008), starspots (Livio & Pringle 1994)) with respect to the L1 point by a differential rotation of the lobe-filling donor (Scharlemann 1982). It can cyclically modify the donor's mass outflow and the mass transfer to the disk. The brightenings caused by the TVI or the mass transfer bursts were superimposed on this cycle length of about 435 d.

We found vastly discrepant values of  $\tau_{\rm D}$  for various brightening episodes of V1363 Cyg. The quantity  $\tau_{\rm D}$  is an essential parameter that helps resolve various processes governing the event. We interpret bumps No. 1, 3, and 4 with the smallest and mutually similar values (or the upper limits) of  $\tau_{\rm D}$  (Fig. 4) as a propagation of the cooling front in the disk finishing the DN outburst (Smak 1984; Hameury et al. 1998). In this context, event 4 (Fig. 2a) is not a simple DN outburst. We interpret its initial decay phase as a propagation of the cooling front similar to events 1 and 3. A significant flattening and undulations in the more advanced part of the decay can be explained by an increase of the mass outflow from the donor's nozzle due to its irradiation in the advanced outburst phase (see the model of Hameury et al. (2000)).

A comparison of the mutually similar values of  $\tau_D$  of events 1, 3, and 4 with the position of V1363 Cyg in the  $\tau_D$ - $P_{\rm orb}$  diagram for DNe (Fig. 4) indicates its  $P_{\rm orb}$  about 20–40 hr, provided that the TVI causes them and obeys the Bailey relation (Bailey 1975). Also, the peak magnitude of V1363 Cyg (the tail of the histogram in Fig. 3b) shows

that this CV would be located in the TVI region all the time if its  $P_{\text{orb}}$  were longer than about 20 hr (Fig. 6).

On the contrary, the divergent and remarkably high values of  $\tau_{\rm D}$  of the broad events 2 and 5 (discrete brightening episodes still in the TVI region) need modification of the cooling front propagation for these two cases. Event 2 was roughly similar (although shorter) to a specific state of activity (several very broad bumps (the longest one 600 d) in the light curve) of the post-nova X Ser (Honeycutt et al. 1998) (the x symbol in Fig. 6). Such bumps in X Ser (Honeycutt et al. 1998), occurring among DN outbursts (Šimon 2018), had the peak  $M_{\rm opt}$  still inside the TVI region (i.e., below an extrapolation of the maxima's peaks of DNe with  $P_{\rm orb}$  (Patterson 2011)) (Fig. 6). A decrease of  $M_{\rm opt}$  of a post-nova containing the disk with time thus may not always be regular and irreversible.

A variation of  $\dot{m}_{\rm tr}$  in a given DN does not lead to a change of  $\tau_{\rm D}$  of the DN outbursts (Buat-Ménard et al. 2001). However, irradiating the disk by the hot WD in a post-nova can modify the situation. Schreiber et al. (2000) show that even if the accretion rate in such a CV is low enough to permit TVI, disk irradiation from the very hot WD suppresses DN outbursts for about a century since the CN outburst. Using this model, we assume that the irradiated disk remains in the hot state during a significant part of the decaying branch of the DN outburst. Its optical flux will decay as the disk's mass decreases because accretion onto the WD will diminish with the outburst progress. The broad brightening episodes with slow decays can thus be caused both in the post-novae V1363 Cyg and X Ser and keep the disk in the hot state for a big part of the decay of the DN outburst.

In the interpretation, the remarkably low values of  $\tau_{\rm D}$  of events 2 and 5 show that the structural changes of the disk that can modify its irradiation by the hot WD may be significant only in part of the outbursts in V1363 Cyg. The changes of the disk influencing this irradiation can occur with various strengths all the time, as indicated by the quiescent (out of the outbursts) brightness variations (Figs. 1 and 5). The activity of the active regions on the secondary component mentioned above may contribute to the modification of mass flow to the disk with time. The repeated observing of the variations of the orbital modulation in V1363 Cyg can help assess the structural changes of the disk and their variations. Such irradiated disk also deserves further modeling.

The absence of DN outbursts in most post-novae with  $P_{\rm orb} < 8\,{\rm hr}$  in the zone of  $M_{\rm opt}$  of V1363 Cyg (Fig. 6) shows that these systems reside on the peak magnitude of the outbursting DNe with the disk ionized out to its outer rim because of a high  $\dot{m}_{\rm tr}$  (Hameury et al. 1998). Also, the

position of the recurrent nova U Sco in Fig. 6 similar to that of GK Per between its quiescence and outburst peak is evidence that the post-novae can reside without the DN outbursts in the TVI zone. In the context of the activity of V1363 Cyg and other post-novae, irradiation from the cooling WD play a significant role in the post-nova evolution and the character of activity (Schreiber & Gänsicke 2001). This WD remains very hot ( $T_{\rm eff}$  a few  $\times 10^5$  K) after the nova explosion. This value only gradually decreases with time (Prialnik 1986). If the disk is subject to the TVI in the absence of irradiation, strong irradiation by the WD can suppress the TVI, while a weaker one gives rise to an inner steady-state disk region, surrounded by a TVI unstable outer annulus (Mineshige et al. 1990; Schreiber et al. 2000; Schreiber & Gänsicke 2001).

In addition, the peak  $M_{\rm opt}$  (including event 2) of V1363 Cyg was only about 1 mag lower than those of the binary supersoft X-ray source (BSXS) QR And (Beuermann et al. 1995) and some V Sge-type CVs (Steiner & Diaz 1998). In the models of van den Heuvel et al. (1992); van Teeseling & King (1998); Ginzburg & Quataert (2021), irradiation of the companion in BSXS can invoke a very high  $m_{\rm tr}$ . It may be at a self-sustaining rate of about  $10^{-7}{\rm M}_{\odot}\,{\rm yr}^{-1}$  for up to a thousand years since the CN outburst in some cases (Ginzburg & Quataert 2021). According to Steiner & Diaz (1998), some V Sge-type CVs may be the optical counterparts of BSXSs.

Extensive changes in the activity after the CN outbursts are observed in some CVs (Livio 1987). The features consistent with the DN outbursts (the TVI already operating) appear at least intermittently, mainly in the later phases (years, decades) of the slow decay of the mean luminosity of some post-novae (e.g., V446 Her (Stienon 1971; Honeycutt et al. 2011); BK Lyn (Patterson et al. 2013); GK Per (Hudec 1981; Sabbadin & Bianchini 1983) X Ser (Šimon 2018)). It suggests that they contain the accretion disks able to switch from the hot (ionized) state to the TVI regime and produce the DN outbursts during the years or decades since the finish of the CN outburst. V1363 Cyg appears to be already in the TVI region, too.

There are also some other CVs that have observable shells suggesting a CN outburst in the system in the past: Z Cam, the limit of 1300 years since the CN outburst (Shara et al. 2012), AT Cnc with the CN outburst about 330 years ago (Shara et al. 2017a), Nova Sco 1437 (Shara et al. 2017b). It constrains the upper limit of the time elapsed since the nova outburst also for V1363 Cyg. The DN outbursts show that these post-novae are already in the TVI zone. The CN explosion of V1363 Cyg was thus a relatively recent event.

#### **Acknowledgments**

This study was supported by the EU project H2020 AHEAD2020, grant agreement 871158. Also, support by the project RVO:67985815 is acknowledged. This research used the observations from the AAVSO International database (USA). I acknowledge with thanks the variable star observations from the AAVSO International Database contributed by observers worldwide and used in this research.

#### References

Bailey, J. 1975, Journ. Brit. Astr. Ass., 86, 30

Bailer-Jones, C. A. L., Rybizki, J., Fouesneau, M., Mantelet, G., & Andrae, R. 2018, AJ, 156, 58

Bateson, F. M. 1974, PVSS, 2, 1

Beuermann, K., et al. 1995, A&A, 294, L1

Bode, M. F., & Evans, A. 1989, Classical novae, edited by M. F. Bode and A. Evans. ISBN 978-0-521-84330-0 (HB). Pp. 16+341, published by Wiley, Chichester, UK

Bos, M., Retter, A., McCormick, J., & Velthuis, F. 2001, IAUC, 7610, 2

Brockwell, P. J., & Davis, R. A. 1987, Time Series: Theory and Methods, Springer-Verlag New York Inc.

Bruch, A., Fischer, F. -J., & Wilmsen, U. 1987, A&AS, 70, 481

Bruch, A., & Schimpke, T. 1992, A&AS, 93, 419

Buat-Ménard, V., Hameury, J.-M., & Lasota, J.-P., 2001, A&A, 369, 925

Cannizzo, J. K. 1994, ApJ, 435, 389

Cieslinski, D., Diaz, M. P., & Steiner, J. E. 1999, AJ, 117, 534Collins, P., et al. 1992, IAUC, 5454, 1

Crampton, D., Cowley, A.P., & Fisher, W.A. 1986, ApJ, 300, 788

Dantona F., & Mazzitelli I., 1982, ApJ, 260, 722

Della Valle, M., Pasquini, L., Daou, D., & Williams, R. E. 2002, A&A, 390, 155

De Young James, A., & Schmidt Richard, E. 1994, ApJ, 431, L47

Diaz, M. P., & Steiner, J. E. 1989, ApJ, 339, L41

Diaz, M. P., & Steiner, J. E. 1995, AJ, 110, 1816

Drake, A. J. et al. 2009, ApJ, 696, 870

Duerbeck, H. W. 1981, PASP, 93, 165

Duerbeck, H. W., & Seitter, W. C. 1990, LNP, 369, 165

Gaia Collaboration: Brown A. G. A. et al. 2018, A&A, 616, A1 Garcia, Jaime Ruben 2000, JAVSO, 29, 19

Ginzburg, Sivan, & Quataert, Eliot 2021, MNRAS, 507, 475 Green Gregory, M. et al. 2018, MNRAS, 478, 651

Greiner, J., & Wenzel, W. 1995, A&A, 294, L5

Hameury, Jean-Marie, Menou, Kristen, Dubus, Guillaume, Lasota, Jean-Pierre, & Hure, Jean-Marc 1998, MNRAS, 298, 1048

Hameury J.-M., Lasota J.-P., & Warner B. 2000, A&A, 353, 244

Herbig, G. H., Preston, G. W., Smak, J., & Paczynski, B. 1965, ApJ, 141, 617

Honeycutt, R. K., Robertson, J. W., & Turner, G. W. 1998, AJ, 115, 2527

Honeycutt, R. K., Robertson, J. W., & Kafka, S. 2011, AJ,

141, 121

Hsi, T.-T. 1958, Smithson. Contr. Astrophys., 2, 109

Hudec, R. 1981, Bull. Astron. Inst. Czechosl., Vol. 32, 93

Kafka, S., Tappert, C., Honeycutt, R. K., & Bianchini, A. 2003, AJ, 126, 1472

Kafka, S., Ribeiro, T., Baptista, R., Honeycutt, R. K., & Robertson, J. W. 2008, ApJ, 688, 1302

Kafka, S. 2019, Observations from the AAVSO International Database, http://www.aavso.org

Kafka, S. 2021, Observations from the AAVSO International Database, http://www.aavso.org

Kolobow, Craig, & Sion, Edward 2011, PASP, 123, 892

Krautter, J., et al. 1984, A&A, 137, 307

Leavitt, H. 1908, Harv. Circ. 142

Liller, W., & Overbeek, M. D. 1983, IAUC, 3764, 1

Livio, M. 1987, ComAp, 12, 87

Livio, M., & Pringle, J. E. 1994, ApJ, 427, 956

Lomb, N. R. 1976, Ap&SS, 39, 447

McLaughlin, Dean B. 1946, PASP, 58, 46

McLaughlin, Dean B. 1948, PASP, 60, 265

Miller, W. J. 1971, RA, 8, 167

Mineshige, S., Tuchman, Y., & Wheeler, J. C. 1990, ApJ, 359,  $176\,$ 

Munari, U., Moretti, S., & Maitan, A. 2020, A&A, 639, L10 Orosz, Jerome A., Thorstensen, John R., & Kent Honeycutt, R. 2001, MNRAS, 326, 1134

Pagnotta, Ashley, et al. 2015, ApJ, 811, 32

Patterson, J., Schwartz, D. A., Pye, J. P., Blair, W. P., Williams, G. A., & Caillault, J.-P. 1992, ApJ, 392, 233

Patterson, Joseph  $\,$  2011, MNRAS, 411, 2695

Patterson, Joseph et al. 2013, MNRAS, 434, 1902

Pearson, K. J., Wynn, G. A., & King, A. R. 1997, MNRAS, 288, 421

Podsiadlowski, Ph., Han, Z., & Rappaport, S., 2003, MNRAS, 340, 1214

Prialnik, D. 1986, ApJ, 310, 222

Ringwald, F. A., Thorstensen, J. R., Honeycutt, R. K., & Robertson, J. W. 1996, MNRAS, 278, 125

Ringwald, F. A., Chase, Daniel W., & Reynolds, David S. 2005, PASP, 117, 1223

Ritter, H., & Kolb, U. 2003, A&A, 404, 301

Sabbadin, F., & Bianchini, A. 1983, A&AS, 54, 393

Salazar, Irene V., LeBleu, Amy, Schaefer, Bradley E., Landolt, Arlo U., & Dvorak, Shawn 2017, MNRAS, 469, 4116

Sahman, D. I., Dhillon, V. S., Knigge, C., & Marsh, T. R. 2015, MNRAS, 451, 2863

Samus, N. N., Kazarovets, E. V., Durlevich, O. V., Kireeva, N. N., & Pastukhova, E. N. 2017, General Catalogue of Variable Stars: Version GCVS 5.1, Astronomy Reports, vol. 61, No. 1, pp. 80-88

Scharlemann, E. T. 1982, ApJ, 253, 298

Schreiber, M. R., Gänsicke, B. T., & Cannizzo, J. K. 2000, A&A, 362, 268

Schreiber, M. R., & Gänsicke, B. T. 2001, A&A, 375, 937

Schaefer, Bradley E., & Ringwald, F. A. 1995, ApJ, 447, L45

Schaefer, Bradley E., & Collazzi, Andrew C. 2010, AJ, 139, 1831

Shara, Michael M., Mizusawa, Trisha, Zurek, David, Martin, Christopher D., Neill, James D., & Seibert, Mark 2012, ApJ, 756, 107

Shara, Michael M., Drissen, Laurent, Martin, Thomas, Alarie, Alexandre, & Stephenson, F. Richard 2017a, MNRAS, 465, 739

Shara, M. M. et al. 2017b, Natur, 548, 558

Shears, J., & Poyner, G. 2010, JBAA, 120, 169

Šimon, V. 2000a, A&A, 354, 103

Šimon, V. 2000b, A&A, 364, 694

Šimon, V. 2002, A&A, 382, 910

Šimon, V. 2018, A&A, 614, A141

Šimon, V. 2021, The Golden Age of Cataclysmic Variables and Related Objects V. 2-7 September 2019. Palermo, Italy. published February 25, 2021. Online at https://pos.sissa.it/cgi-bin/reader/conf.cgi?confid=368, id 37

Smak, J. 1984, Acta Astron., 34, 161

Stienon, F. M. 1971, PASP, 83, 363

Steiner, J. E., & Diaz, M. P. 1998, PASP, 110, 276

Szkody, Paula, Everett, Mark E., Howell, Steve B., Landolt, Arlo U., Bond, Howard E., Silva, David R., & Vasquez-Soltero, Stephanie 2014, AJ, 148, 63

Thorstensen, J. R., & Taylor, C. J. 2000, MNRAS, 312, 629

van den Heuvel, E. P. J., Bhattacharya, D., Nomoto, K., & Rappaport, S. A. 1992, A&A, 262, 97

van Teeseling, A., & King, A. R. 1998, A&A, 338, 957

Vogt, N., & Breysacher, J., 1980, ApJ, 235, 945

Warner, B. 1987, MNRAS, 227, 23

Warner, B. 1995, Cataclysmic Variable Stars, Cambridge Univ. Press, Cambridge

Watson, M. G., King, A. R., & Osborne, J. 1985, MNRAS, 212, 917

Williams, R. E., Sparks, W. M., Gallagher, J. S., Ney, E. P., Starrfield, S. G., & Truran, J. W. 1981, ApJ, 251, 221

Williger, G., Berriman, Graham, Wade, Richard A., & Hassall, B. J. M. 1988, ApJ, 333, 277